Wiley Online Library
Early View publication on www.wileyonlinelibrary.com
(issue and page numbers not yet assigned;
citable using Digital Object Identifier – DOI)

Phys. Status Solidi A, 1–9 (2016) / DOI 10.1002/pssa.201600178

Part of Topical Section on
Recent Advances in Diamond Science and Technology

physica status solidi a
www.pss-a.com
applications and materials science

Monitoring of nanodiamonds in human urine using artificial neural networks

Kirill Laptinskiy*[,1,2], Sergey Burikov[1,2], Sergey Dolenko[2], Alexander Efitorov[2,3], Olga Sarmanova[1], Olga Shenderova[4], Igor Vlasov[3,5], and Tatiana Dolenko[1,2,3]

[1] Physical Department, M. V. Lomonosov Moscow State University, 119991 Moscow, Russia
[2] D. V. Skobeltsyn Institute of Nuclear Physics, M. V. Lomonosov Moscow State University, 119991 Moscow, Russia
[3] National Research Nuclear University MEPhI, 115409 Moscow, Russia
[4] Adámas Nanotechnologies, Inc., 8100 Brownleigh Dr, Suit 120, Raleigh, NC 27617, USA
[5] A. M. Prokhorov General Physics Institute, Russian Academy of Sciences, 119991 Moscow, Russia

Received 21 March 2016, revised 26 August 2016, accepted 13 September 2016
Published online 28 September 2016

Keywords artificial neural networks, diamond, fluorescence, nanomaterials, urine

* Corresponding author: e-mail laptinskij@physics.msu.ru, Phone: +7 495 939 16 53, Fax: +7 495 939 11 04

This paper presents the results of application of the elaborated methods for monitoring of nanodiamonds in human urine using fluorescence spectroscopy. High efficiency of artificial neural networks applied for recognition and estimation of the concentration of nanodiamonds in urine with a strong autofluorescence background is demonstrated. It was found that minimal concentration of nanodiamonds with strong fluorescence containing nitrogen-vacancy (NV) centers can be detected in urine by fluorescence spectroscopy at a level of 3.06×10^{-4} g L^{-1}; while use of artificial neural networks for detection of weakly fluorescent detonation nanodiamonds provides reasonably high accuracy of detection, not worse than 6.8×10^{-3} g L^{-1}.

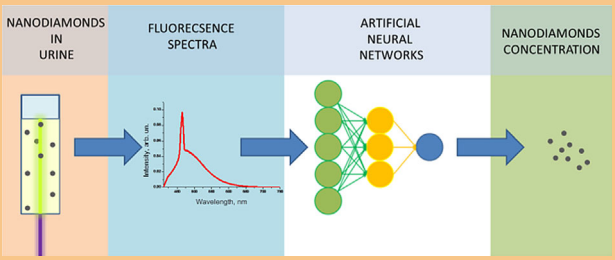

1 Introduction Theranostics is one of the hot topics in modern biomedicine. A general goal is to create a nanocarrier combining an opportunity for tissue diagnostics and an ability to provide a therapeutic effect. Nanodiamonds (ND) are a promising material to accomplish this goal [1–11]. Combining such properties as stable luminescence, polyfunctionality of the surface which can be specifically modified, active sorption properties, non-toxicity and biocompatibility, NDs have triggered a high level of interest for their application in biomedicine.

Biomedical applications of ND as fluorescent biomarkers [1–3, 8, 11] including visualization of processes in cells [5, 8, 9], as a drug carrier and sorbent of toxic elements [4, 6, 7, 10, 11] have been reported. Typically for biomedical applications, the surfaces of NDs are modified [12, 13] or covered with a shell [14–19] such as, for example, mesoporous silica shell [15, 16] or copolymers [17–19], which have, besides fluorescence properties, higher biocompatibility and higher ability to adsorb and retain medical drugs in comparison with ND. Using aminated and carboxylated NDs, the authors [20] demonstrated controlled release of the drugs tetracycline and vancomycin by changing the pH. In the article [21], the neuroprotective effect of nanodiamonds in Alzheimer's disease was shown. The authors of Ref. [22] reported application of nanodiamonds for curing gum disease, for healing of skin, and exfoliation of damaged skin in the case of sunburns or scar tissue. Various groups investigated the role of NDs as anticancer drug delivery systems [23, 24]. With that being said, one can conclude

that nanodiamonds are a very promising material in medical applications.

Nevertheless, practical application of ND as fluorescent biomarkers and drug carriers is closely related with the problem of optical visualization of nanoparticles in biotissue. At present, the most common method is optical visualization using fluorescence [25–27]. A serious problem in such studies is the background fluorescence due to the fluorescence of inherent fluorophores in biological tissue – tryptophan, phenylalanine, tyrosine, collagen, flavins, beta-carotene, porphyrins, vitamins, etc.

The autofluorescence spectrum of the tissue is the result of superposition of fluorescent bands of many tissue fluorophores, and it extends from 200 to 750 nm [26]. Such autofluorescence significantly hampers observation of the occurring processes and the motion of fluorescent nanoparticles. That is why the problem – how to get rid of the background fluorescence – is a very urgent one. Methods of extraction of the fluorescent signal of nanoparticles-markers in the presence of the autofluorescence background of biological tissue, and control of the change in fluorescence intensity needs to be further elaborated. Obviously, these methods are necessary for testing theranostic nanoparticles: it is required not only to keep track of biomarkers and drug carriers, but also to control their distribution (and concentration) in specific organs, and also to monitor the rate and efficiency of excretion of nanoparticles from the organism.

At present, the problem of fighting background fluorescence is solved basically by the following methods: (i) in the field of materials science, by development of nanoparticles with optimal optical properties, by elaboration of methods of targeted modification of their surface and of synthesis of nanocomposites for providing or enhancing the required properties [14–19, 28]; (ii) in the field of experimental technique, by focusing the exciting laser radiation in a very small volume in order to reduce the background signal, i.e., by improvement of the rather expensive equipment [29, 30]. In both cases, there exists the problem of taking into account interactions among nanoparticles themselves and with surrounding bioenvironmental, which is still far from its solution.

The authors of this paper suggested using methods of intelligent data analysis, namely, artificial neural networks (ANN), for elaboration of optical visualization of nanoparticles in biotissue [31, 32].

ANN is one of the most powerful algorithms of data analysis providing efficient solution of pattern recognition problems and of multi-parameter inverse problems in many areas, including optical spectroscopy [31–36]. Adaptive methods of data analysis are used today in almost all fields of bioinformatics [31], as here there is often lack of adequate physical or mathematical models describing the studied objects. Solving such problems as selection of genome fragments, classification of proteins, recognition of transmembrane helixes, identification of signal peptides, etc. [36], recognition of diseased tissues by their modified fluorescence [33, 34] using ANN is now very promising.

A proof of principle separation of the fluorescence signal of carbon nanoparticles from the autofluorescence of egg protein using artificial neural networks has been demonstrated for the first time [37, 38]. Besides that, quantitative threshold of sensitivity of the method has been determined: estimation of minimal concentration of nanoparticles (when the presence of nanoparticles can be detected confidently against the background of autofluorescence of biotissue) has been obtained with the help of ANN.

In this study, the methods for monitoring of theranostic nanoparticles in human urine using fluorescence spectroscopy were elaborated. Such optical visualization of ND is the main stage of control of efficiency of excretion of nanoparticles from the human body. Accuracies of determination of concentrations of two types of nanodiamonds in urine have been determined, namely for nanodiamonds with fluorescent nitrogen-vacancy (NV) centers (by their calibration dependencies) and for detonation nanodiamonds (by neural network algorithms). Use of the neural network technique as a high efficiency method for recognition and estimation of the concentration of detonation nanodiamonds in urine is demonstrated.

2 Experimental

2.1 Materials Two types of nanodiamonds with different fluorescent properties were used: nanodiamonds with NV-centers (ND-NV) and detonation nanodiamonds (DND).

Nanodiamonds with NV centers were obtained by milling of the 15 μm diamonds synthesized by the HPHT method. The milled particles were irradiated with a 2 MeV electron beam; the obtained dose was 5×10^{18} e cm^{-2}. Then the particles were annealed for 1 h at 850 °C and ground in a mill with zirconium beads. The resulting particles were cleaned by HF and separated into fractions in a centrifuge. As a result of fractionation, 100 nm ND with NV-centers were separated. The studied ND-NV samples were not further modified.

DND was synthesized by explosion of mixture of trinitrotoluene (TNT) and 1,3,5-trinitrotoluene-1,3,5-x-triturate (RDX) in a gas cooling media. DND was separated from the soot by using a mixture of sulfuric/nitric acids with addition of sodium oleate (this work was performed at NPO Altay, Russia). As a result of further milling and fractionation, the fraction of DND with size 5 nm was separated. One should note that during treatment of the soot in the mixture of sulfuric and nitric acids, groups of oxidized graphite can be formed on the DND surface. Then the surface of the separated DND particles was modified with carboxylic groups by treatment of DND in air at 420 °C for a period of 1 h.

ND suspensions in urine diluted 10 times were prepared with DND concentrations varying from 0 up to 0.2 g L^{-1} in increments of 0.01 g L^{-1}; the concentration of ND-NV was

changed from 0 to 0.02 g L^{-1} in increments of 0.001 g L^{-1}. Choice of the ND concentration range was based upon experiments conducted in diluted urine was used, and in real urine the maximal concentrations used was 2 and 0.2 g L^{-1} (corresponding to safe working concentrations for biomaterial [2, 3, 39]). Urine samples were taken from 15 healthy donors (both male and female) in different age groups (19–50 years), with their consent.

2.2 Experimental setup Fluorescence and Raman spectra of samples were measured using a laser spectrometer. For excitation of fluorescence of detonation ND, a diode laser (wavelength 405 nm, output power 100 mW) was used; argon laser (wavelength 514.5 nm, output power 200 mW) was used for excitation of fluorescence of ND-NV samples. Fluorescence spectra were measured using a monochromator (Acton, grade 1800 grooves/mm, focal length 500 mm) and a photomultiplier (Hamamatsu, H-8259-01) in the spectral range 400–750 nm, with practical resolution of 0.5 nm. The temperature of the samples was stabilized at 20.0 ± 0.1 °C with the help of a special thermostabilized cuvette. The obtained spectra were corrected to spectra acquisition time and to laser power, and then normalized by the area under the curve of water Raman valence band.

Spectra of the IR absorption of the samples were measured using a Varian 640-IR FT-IR spectrometer equipped with an attenuated total reflection cell with a ZnSe crystal. The spectral resolution was 4 cm^{-1}.

3 Results and discussion

3.1 Fluorescence properties of ND-NV in urine. The method for determination of ND-NV concentration in urine by fluorescence spectra In Fig. 1, the obtained Raman and fluorescence spectra of urine and suspensions of ND-NV in water and urine at the same concentration of 0.02 g L^{-1} are presented. The band with maximum near 623 nm corresponds to valence vibrations of water OH-groups. Zero-phonon lines near 575 and 637 nm testify that in the studied ND samples, two types of nitrogen vacancies are present: $-NV^0$ and NV^-. As fluorescence of ND-NV is caused by NV-centers located deep in the bulk of ND, interactions of surrounding molecules with surface groups of ND cause no significant influence on the intensity of ND fluorescence. Besides this urine fluorescence at excitation by radiation with wavelength 514.5 nm is rather weak, while NDs with NV centers have intense fluorescence; that is why extraction of the fluorescence signal of ND-NV from the background urine fluorescence is not a problem.

For a quantitative description of the fluorescence of ND in suspensions, parameter F_0 was used. It is the ratio of the integral intensity of fluorescence and integral intensity of the water Raman valence band [40, 41].

To solve the problem of determination of the concentration of ND-NV in urine using Raman and fluorescence spectra of suspensions for all spectra of urine and of suspensions of ND-NV in water and in urine in he mentioned range of concentrations of ND-NV (0–0.02 g L^{-1}), parameters F_{0NV} were calculated (Fig. 1). In this case, the parameters F_{0NV} were calculated for integral intensity of fluorescence in the range from 641 up to 800 nm where urine fluorescence is negligible in order to exclude its influence on the spectrum of ND-NV fluorescence (Fig. 1).

For diagnostic purposes (e.g., to determine the number of particles), such a calculation is entirely acceptable. The obtained concentration dependencies $F_{0NV}(C)$ are shown in Fig. 2. As one can see in Fig. 2, these dependencies can be well approximated by linear functions. Due to the way of calculation of F_{0NV}, the straight lines $F_{0NV}(C)$ for the samples of urine from various donors are close to each other, and they even do not differ much from the dependence $F_{0NV}(C)$ for the suspensions of ND-NV in water. This provides practically equal accuracy of determination of

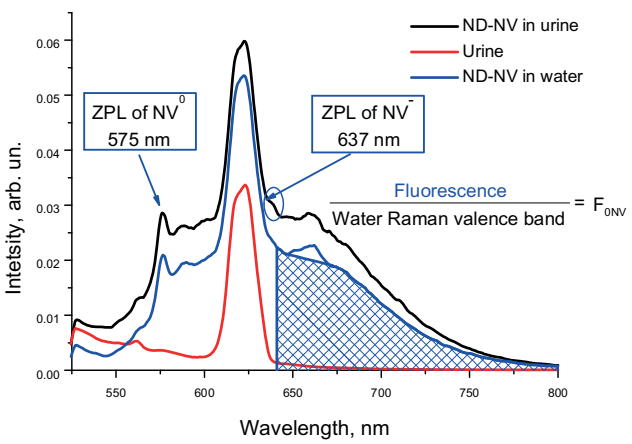

Figure 1 Raman and fluorescence spectra of urine, ND-NV suspensions in water and urine with concentration 0.02 g L^{-1}. Illustration of calculation of the parameter F_{0NV}.

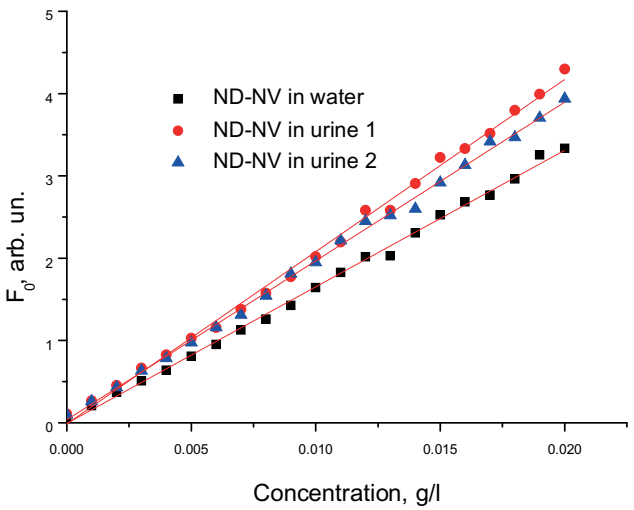

Figure 2 The dependences of parameter F_{0NV} on the concentration of ND-NV in urine samples and in water. Root mean square errors are equal to: 0.053 (black), 0.079 (red), 0.058 (blue).

concentration of ND-NV in various samples of urine using the obtained calibration dependencies. As a result of the calculations, it was determined that the accuracy of the ND-NV concentration in water and urine using dependencies $F_{0NV}(C)$ was 2.42×10^{-4} and $3.06 \times 10^{-4}\,g\,L^{-1}$, respectively.

One should note that the achievement of such a high accuracy of determination of ND-NV concentration in water and in urine using fluorescence and Raman spectra was to a large extent due to the choice of the excitation wavelength 514.5 nm. In this case, the Raman valence band of OH-groups, which is the internal benchmark for calculation of parameters F_0, practically does not overlap with the zero-phonon lines (ZPL) of ND-NV. For example, under laser excitation by 488 or 532 nm wavelengths, the valence band of OH-groups significantly overlaps with one of the two ZPL, making correct calculation of parameters F_0 impossible.

3.2 Fluorescence properties of DND in urine The fluorescence of DND is much weaker than the fluorescence of ND with NV centers. DNDs have fluorescence at excitation wavelength 405 nm; at these conditions urine fluorescence is also significant, and fluorescence spectrum of urine overlaps with fluorescence spectrum of DND. Taking into account that DND are much easier and cheaper to produce and have a better perspective from the point of view of surface modification than ND with NV centers, the problem of DND recognition in biotissue by fluorescence spectra is very urgent.

In Fig. 3, fluorescence and Raman spectra of urine and DND suspensions in water and urine with the same concentration $0.2\,g\,L^{-1}$ are presented. The band with a maximum near 464.5 nm corresponds to the valence vibrations of OH-groups of water. As one can see in Fig. 3, fluorescence spectra of DND (from 440 to 580 nm) and urine (from 400 to 700 nm) overlap over a wide spectral range. At the same time, the spectrum of DND in urine is significantly different from superposition of fluorescence spectra of DND and urine. This confirms the existence of strong nonlinear interactions between ND surfaces and biomacromolecules. According to literature data [42], the fluorescence properties of DND are caused by defects on its surface. That is why the signal of DND fluorescence is very sensitive to the environment, since fluorescence of DND can be changed as a result of interaction of DND surface groups with surrounding molecules. Thus, extraction of the fluorescence signal of DND from the background fluorescence of urine is a very difficult problem.

This problem is complicated by high variability of urine fluorescence and, therefore, by fluorescence of DND in urine. In Fig. 4, Raman and fluorescence spectra of diluted urine from various donors are presented. These spectra are significantly different by both position of band maximum (varied between 479 and 510 nm) and by band shape. Variability of spectra of DND fluorescence in urine can be demonstrated using calculated quantitative characteristics of the fluorescence spectra F_0. The method of calculation of F_0 is illustrated in Fig. 5.

Parameter F_0 and differential ΔF_0 were calculated for all Raman and fluorescence spectra of urine and suspensions of DND in water and urine with DND concentration $0.2\,g\,L^{-1}$. To obtain ΔF_0, the value of the F_0 parameter of spectra of solvent (without DND) was subtracted from the F_0 parameter of DND suspension in water or urine, i.e., $\Delta F_0 = F_{0suspension} - F_{0solvent}$. In a rough approximation, one can consider this differential parameter ΔF_0 to be a measure of change of fluorescent properties of DND in different solvents. From a comparison of the values of ΔF_0, obtained for fluorescent spectra of DND suspensions in water and urine samples from each of the 15 donors (Fig. 6), the following conclusions can be made: (i) fluorescence properties of DND significantly increase in urine in comparison with water; (ii) high variability of change in

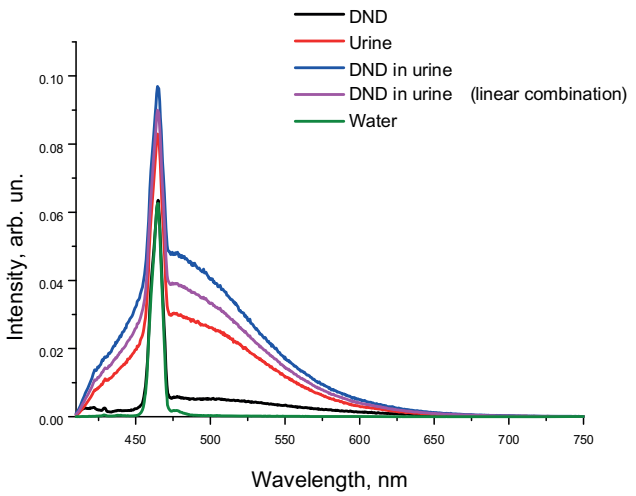

Figure 3 Raman and fluorescence spectra of water, urine, DND suspensions in water and urine; DND concentration $0.2\,g\,L^{-1}$.

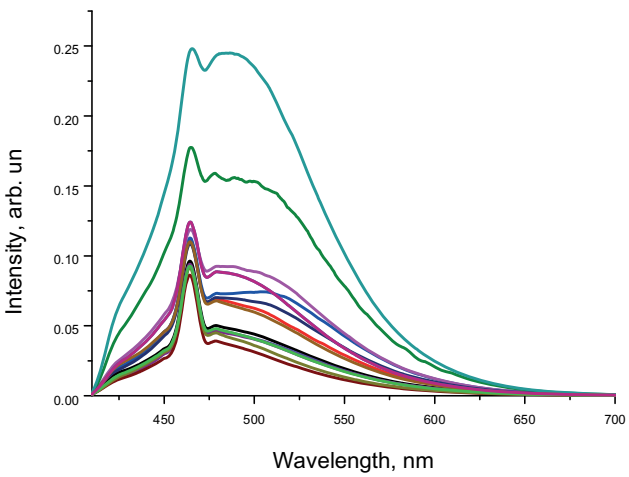

Figure 4 Experimental fluorescence spectra of various samples of diluted urine (without ND).

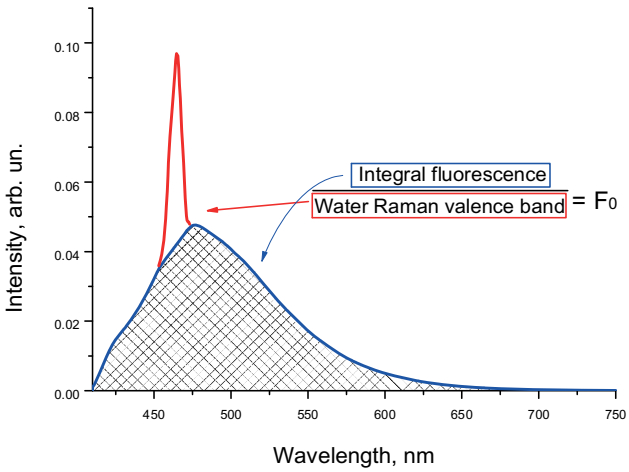

Figure 5 Illustration of calculation of F_0 = integral fluorescence/ integral Raman intensity of water valence band.

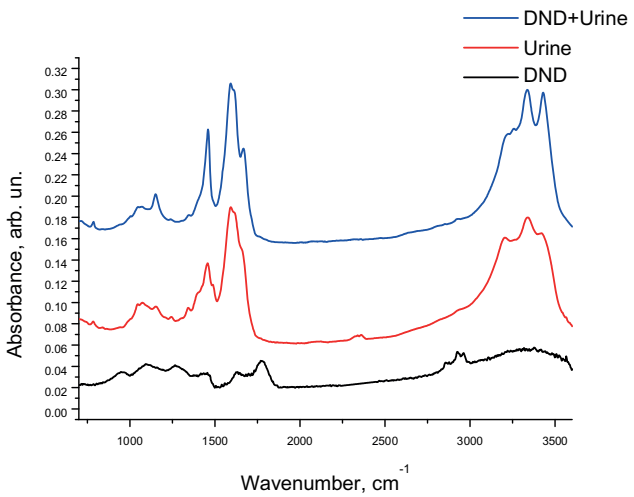

Figure 7 Spectra of IR absorption of evaporated samples of DND (from water), urine and DND evaporated from this urine.

fluorescence properties of DND depending on an urine sample is observed, what confirms once again the existence of significant nonlinear interactions between DND surface groups and biomacromolecules.

Significant interactions of DND and urine molecules are also revealed in the spectra of IR absorption of the studied samples. In Fig. 7, the IR spectra of evaporated samples of DND from water, urine, and DND from this urine, are presented. As one can see, when DND is added to urine, the intensity of the peak caused by rocking vibrations of NH_2 groups (1155 cm^{-1}) decreases, the intensity of the peak near 1460 cm^{-1} caused by asymmetric valence vibrations C–N in CN_2 increases. Change of the ratio of intensities of in-plane (3350 cm^{-1}) and out-of-plane (3440 cm^{-1}) vibrations of NH

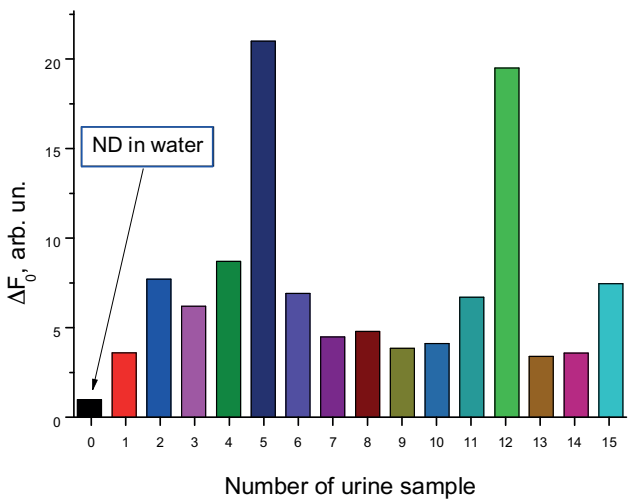

Figure 6 Comparison of the values of differential parameters ΔF_0 for fluorescence of water DND suspension and DND suspension in urine samples of each of the 15 donors (at the concentration of DND equal to 0.2 g L^{-1}).

caused by interactions of DND and urine is also observed in the spectra. The observed changes in IR spectra of urine and DND in urine, as well as the fact that DND fluorescence in urine increases, confirm the hypothesis about surface nature of DND fluorescence [42].

From the above analysis of the fluorescence properties of DND in urine, it follows that elaboration of the method of optical visualization of DND in biotissue, i.e., solution of the inverse problem of extracting DND fluorescence from the background of urine autofluorescence requires application of adaptive methods of data processing [43], in particular, application of the technique of artificial neural networks [32]. Neural network algorithms are able to overcome the high variability of fluorescence properties both of nanoparticles and of biotissue in the studied samples, and also to take into account the significant nonlinear interactions between them.

4 Application of artificial neural networks for recognition of DND in human urine

As it was mentioned above (see Section 3.1), elaboration of a method of optical visualization of DND in biotissue, i.e., solution of the problem of extraction of DND fluorescence against the background of autofluorescence of urine, requires application of adaptive methods of data processing, in particular, of artificial neural networks [32].

4.1 Artificial neural networks

The architecture of the artificial neural networks (ANN) used in this study to solve the described problem, is the most widely known ANN architecture – the multi-layer perceptron (MLP). A basic element that is used to construct any MLP is called a formal neuron. This element has multiple inputs and a single output. Each input is assigned its own weight coefficient, w_j. A non-linear function F (activation function) is applied to the weighted sum of the values x_j at the inputs of the neuron

to form the value y at the output of the neuron:

$$y = F\sum_{j=0}^{N} w_j x_j, \quad x_0 \equiv 1. \tag{1}$$

A number of identical neurons, which differ only by the values of their weights, are united in parallel into a layer. An MLP consists of several layers (Fig. 8); each neuron is linked to all the neurons of the preceding and the next layers (the so-called fully connected scheme). The signal propagates according to Eq. (1) from the inputs of the first layer to the output of the last one.

The first layer of an MLP is used to introduce data into the network, so it is called the input layer. The number of neurons in the input layer corresponds to the number of features characterizing the processed data sample (e.g., the number of channels of a spectrum). The neurons of the input layer are not formal neurons like those described above – they perform no data processing, they just distribute the signal from the input of the network to the neurons of the next layer.

The last layer of an MLP represents the output of the whole network (e.g., the determined ND concentration), so it is called the output layer (Fig. 8). If several quantities are determined simultaneously, there are several neurons in the output layer.

One or several layers located between the input and the output layers are called hidden layers, as they are not directly connected either to the input or to the output of the network. The quantity of neurons in the hidden layer(s) determines the general complexity of the MLP.

The value at the output of an MLP depends not only on the values at its inputs, but also on the weights of all the neurons (Eq. (1)). That is why the weights have to be assigned some correct values to provide correct answers of the network. To achieve that, the network is trained. Training of a MLP is done by evaluation of answers of the MLP on the samples from the training data set with known correct answers, with further adjustment of weights for all neurons. The procedure of training provides minimization of the mean error of the MLP over the training set. Usually this is done by the error backpropagation algorithm [32], which implements minimization of error by gradient descent in the space of weights.

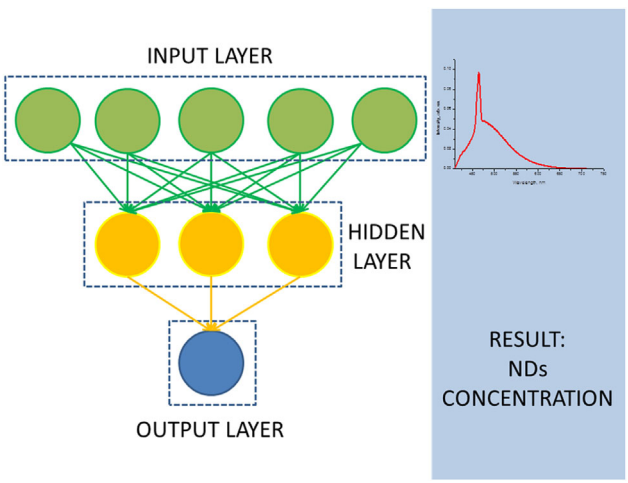

Figure 8 The scheme of a multi-layer perceptron.

In general, one needs three data sets to work with ANN: a training set used to calculate error and adjust weights during training, a test set used to prevent network overtraining (to provide reasonable results on new data), and an examination set used to evaluate the quality of ANN training and to estimate the error of determination of the sought parameters of the solved problem on independent data.

4.2 Extraction of DND fluorescence against the background fluorescence spectrum of urine using ANN When ANN are used to solve inverse problems in optical spectroscopy, three approaches can be used: "model-based," "quasi-model," "experiment-based" [35]. The "model-based" approach requires an analytical model of solution of the direct problem, to compute the data set for ANN training. In the "quasi-model" approach, a small set of experimental data is used to construct a parametric "quasi-model" of input data (spectra); on the base of this "quasi-model" one can compute spectra for training, test and examination sets. In both approaches, the opportunity to compute a large amount of samples provides high representativity of all sets for work with ANN. However, in these cases the accuracy of the solution of the inverse problem significantly depends on how adequate is the chosen analytical model or the constructed "quasi-model" to the studied object, and on how correctly the real noise was taken into account in the experiment.

Within the "experiment-based" approach, the neural network is trained only on experimental data. Obviously in this case it is most often impossible to provide high representativity of all the sets. But this approach has a very important advantage – when ANN is trained on real experimental data, the experimental noise and all molecular interactions in the studied objects are taken into account to a greater extent.

Obviously, the "model-based" and "quasi-model" approaches cannot be used for solution of the problem of extraction of the fluorescence signal of DND against the fluorescence background of urine, because there still is no adequate analytical model describing complex non-linear interactions between molecules of urine and taking into account the high variability of fluorescence properties of urine. That is why in this study the "experiment-based" approach was used.

As it was mentioned above (Section 2.1), in the experiment, 15 series of Raman and fluorescence spectra of DND suspensions in urine were obtained. Every series consisted of spectra of suspensions in the range of DND concentrations from 0 up to $0.2\,\mathrm{g\,L^{-1}}$ with increment $0.01\,\mathrm{g\,L^{-1}}$. To increase stability of the solution of the

problem to the model of biological object, samples of urine from 15 different healthy donors were used. Thus, the total data array consisted of 315 spectra. This array was used to form training, test, and examination sets for ANN training.

The whole obtained array of data was divided into training, test, and examination sets according to the ratio 13:2:1, respectively. The division was performed in two ways: (i) randomly after "mixing" of spectra from all series and (ii) in such a way that each series was completely in one of the three sets ("by whole series").

The problem was solved using a perceptron with a single hidden layer, trained by error backpropagation algorithm [32]. The number of neurons in the hidden layer was set to 8, 16, or 32. The activation function was logistic in the hidden layer and linear in the output layer. The training parameters were the following: learning rate 0.01, learning moment 0.5, random order of sample presentation, training was stopped after 1000 training epochs after minimum error on the test data set.

Table 1 presents exemplary results of application of the perceptron with different number of neurons in the single hidden layer to the examination set, for different methods of division into the sets. As it can be seen from Table 1, the average error of determination of DND concentration in urine on the examination set is nearly the same for both methods of division, and, on the average, it is $6.8 \times 10^{-3}\,\mathrm{g\,L^{-1}}$. This value can be used as an estimate of the detection level of DND in urine.

The best result with minimum error of determination of concentration was obtained by using perceptron with eight neurons in the hidden layer, with division into sets "by whole series": the mean absolute error (MAE) of determination of DND concentration was $5.8 \times 10^{-3}\,\mathrm{g\,L^{-1}}$. This method of division also looks more realistic, as for practical application, each new series should fall completely into the examination set, in order not to retrain the ANN each time.

Thus, despite significant overlapping of fluorescence signals of DND and natural biofluorophores, use of ANN allows detection and estimation of concentration of particles of detonation nanodiamonds in biofluid. Such method is very useful, taking into account that synthesis and purification of DND are cheap and easily available, and that creation of nitrogen vacancies in ND requires expensive equipment and adjusting of conditions of particle preprocessing.

Table 1 Mean absolute error of the ANN in the examination data set.

method of division of the data array	number of neurons in the hidden layer	value of mean absolute error (MAE) in the examination set ($\mathrm{g\,L^{-1}}$)
random after mixing	8	0.0077
	16	0.0077
	32	0.0066
second series as examination set	8	0.0058
third and sixth series as test set	16	0.0071
All the other series as training set	32	0.0075

The obtained values for the error of determination of concentration of excreted nanodiamonds in urine were compared to data for rats, available in the literature. The authors of Ref. [44] made eight ND injections to rats during 4 weeks at 3-day intervals. They injected a water suspension of ND with a concentration of $500\,\mathrm{mg\,L^{-1}}$ at the rate of 4 mg of nanoparticles per 1 kg body weight. According to the results of the studies by the authors of Ref. [45], 90% of the NDs are accumulated in the lung, spleen, and liver and then, the remaining NDs are excreted in the urinary tract. Then the concentration of NDs excreted from rats is $0.1 \times 0.5 = 0.05\,\mathrm{g\,L^{-1}}$. The weight of a human is about 100 times larger. The obtained values for the error of determination of concentration of excreted nanodiamonds in urine are $3.06 \times 10^{-3}\,\mathrm{g\,L^{-1}}$ for ND-NV, and $6.8 \times 10^{-2}\,\mathrm{g\,L^{-1}}$ for DND, thus providing detection of NDs in urine even taking into account the high fraction of particles remaining in organs (90%). It should be noted that at the specified doses, nanodiamonds are not toxic for organs. Thus, the $250–500\,\mathrm{mg\,mL^{-1}}$ doses of injected NDs with 20 and 100 nm size in lung, kidney, colon, and liver human cell lines revealed no cytotoxic or genotoxic effects [46]. Numerous literature data indicate that with time NDs are excreted from the organism [47] The results of the authors [48] have shown that no NDs were found in the mice's liver, spleen, and lymphatic node through histopathological and HRTEM observations, even when the mice were instilled with a much higher dose of $20\,\mathrm{mg\,kg^{-1}}$ NDs.

5 Conclusions In this study, methods of detection and estimation of the quantitative content of detonation nanodiamonds and ND with NV-centers in a real biological object by fluorescence spectra were elaborated. It has been demonstrated that using the dependencies of the fluorescence-derived parameter (F_0) on ND-NV concentration in the suspension, it was possible to determine the concentration of ND-NV in urine by their fluorescence spectra with the accuracy of $3.06 \times 10^{-4}\,\mathrm{g\,L^{-1}}$.

A proof of principle for recognition of the fluorescence signal of DND against the background of urine autofluorescence with the help of artificial neural networks has been demonstrated. It has been shown that the elaborated method allows detection of DND in urine and to determine its concentration with the accuracy (mean absolute error) of $6.8 \times 10^{-3}\,\mathrm{g\,L^{-1}}$ on average.

The advantage of ANN application to the problems of detection of DND in biotissue/biofluids follows from the fact that training of neural networks may be performed on data that takes into account all kinds of interactions of nanoparticles with biomacromolecules, and with account for experimental noise of various natures. At the given stage, this method can be used when DND are injected into the

skin, surface vessels, blood. One should note that such application of ANN is very promising in other fields of work with ND, for example, when excitation of biotissue with ND is performed by X-ray sources or acoustic methods.

Acknowledgements The following parts of this study were supported by the following foundations: (i) elaboration of methodology and application of ANN to solve the studied inverse problem (A.O.E., S.A.D.) have been performed at the expense of the grant of Russian Science Foundation (project no. 14-11-00579); (ii) planning and conducting of the experiment, discussion of physical results (T.A.D., I.I.V., S.A.B., K.A.L.) were supported by the grant of the Russian Foundation for Basic Research no. 15-29-01290 ofi_m; and (iii) planning of the experiment, characterization of samples, discussion of results were supported by the Competitiveness Programm of NRNU MEPhI (T.A.D., I.I.V., A.O.E.). O.S. acknowledges support from the contract HHSN268201500010C from NIH, NIHLBI for fluorescent NDs production.

References

[1] V. N. Mochalin, O. A. Shenderova, D. Ho, and Yu. Gogotsi, Nature Nanotechnol. **201**, 1 (2011).
[2] A. P. Puzyr, A. V. Baron, K. V. Purtov, E. V. Bortnikov, N. N. Skobelev, O. A. Mogilnaya, and V. S. Bondar, Diam. Relat. Mater. **16**, 2124 (2007).
[3] A. M. Schrand, S. A. Hens, and O. A. Shenderova, Crit. Rev. Solid State **34**, 18 (2009).
[4] H. Huang, E. Pierstorff, E. Osawa, and D. Ho, Nano Lett. **7**, 3305 (2007).
[5] M. F. Weng, S. Y. Chiang, N. S. Wang, and H. Niu, Diam. Relat. Mater. **18**, 587 (2009).
[6] M. Chen, E. D. Pierstorff, R. Lam, S. Y. Li, H. Huang, E. Osawa, and D. Ho, ACS Nano **3**, 2016 (2009).
[7] J. Li, Y. Zhu, W. Li, X. Zhang, Y. Peng, and Q. Huang, Biomaterials **31**, 8410 (2010).
[8] C. C. Fu, H. Y. Lee, K. Chen, T. S. Lim, H. Y. Wu, P. K. Lin, P. K. Wei, P. H. Tsao, H. C. Chang, and W. Fann, Proc. Natl. Acad. Sci. USA **104**, 727 (2007).
[9] N. Mohan, C. S. Chen, H. H. Hsieh, Y. C. Wu, and H. C. Chang, Nano Lett. **10**, 3692 (2010).
[10] L.-C. L. Huang and H.-C. Chang, Langmuir **20**, 5879 (2004).
[11] T. A. Dolenko, S. A. Burikov, K. A. Laptinskiy, T. V. Laptinskaya, J. M. Rosenholm, A. A. Shiryaev, A. R. Sabirov, and I. I. Vlasov, J. Alloys Compds. **586**, S436 (2014).
[12] A. Krueger, Chem. Eur. J. **14**, 1382 (2008).
[13] K. K. Liu, W. W. Zheng, C. C. Wang, Y. C. Chiu, C. L. Cheng, Y. S. Lo, C. Chen, and J. I. Chao, Nanotechnology **21**, 315106 (2010).
[14] J. M. Rosenholm, I. I. Vlasov, S. A. Burikov, T. A. Dolenko, and O. A. Shenderova, J. Nanosci. Nanotechnol. **15**, 959 (2015).
[15] E. von Haartman, H. Jiang, A. A. Khomich, J. Zhang, S. A. Burikov, T. A. Dolenko, J. Ruokolainen, H. Gu, O. A. Shenderova, I. I. Vlasov, and J. M. Rosenholm, J. Mater. Chem. B **1**, 2358 (2013).
[16] N. Prabhakar, T. Nareoja, E. von Haartman, D. S. Karaman, H. Jiang, S. Koho, T. Dolenko, P. Hanninen, D. I. Vlasov, V. G. Ralchenko, S. Hosomi, I. I. Vlasov, C. Sahlgren, and J. M. Rosenholm, Nanoscale **5**, 3713 (2013).
[17] I. Rehor, J. Slegerova, J. Kucka, V. Proks, V. Petrakova, M.-P. Adam, F. Treussart, S. Turner, S. Bals, P. Sacha, M. Ledvina, A. M. Wen, N. F. Steinmetz, and P. Cigler, Small **10**, 1106 (2014).
[18] H. Kim, H. B. Man, B. Saha, A. M. Kopacz, O.-S. Lee, G. C. Schatz, D. Ho, and W. K. Liu, J. Phys. Chem. Lett. **3**, 3791 (2012).
[19] X. Q. Zhang, M. Chen, R. Lam, X. Xu, E. Osawa, and D. Ho, ACS Nano **3**, 2609 (2009).
[20] J. Giammarco, V. Mochalin, J. Haeckel, and Y. Gogotsi, J. Colloid Interface Sci. **468**, 253 (2016).
[21] S. Alawdi, E. El-Denshary, M. Safar, H. Eidi, M.-O. David, and M. A. Abdel-Wahhab, Mol. Neurobiol. **53**, 83 (2016).
[22] J. Sung and J. Lin, Diamond Nanotechnology: Synthesis and Applications (Pan Stanford Publishing Pte. Ltd., Singapore, 2010), pp. 137–191.
[23] G. Xi, E. Robinson, B. Mania-Farnell, E. F. Vanin, K. W. Shim, T. Takao, E. V. Allender, C. S. Mayanil, M. B. Soares, D. Ho, and T. Tomita, Nanomedicine: NBM **10**, 381 (2014).
[24] H. B. Man, H. Kim, H.-J. Kim, E. Robinson, W. K. Liu, E.K-H. Chow, and D. Ho, Nanomedicine: NBM **10**, 359 (2014).
[25] R. Jianghong, D.-A. Anca, and Y. Hequan, Curr. Opin. Biotechnol. **18**, 17 (2007).
[26] M. Zellweger, Fluorescence Spectroscopy of Exogenous, Exogenously-Induced and Endogenous Fluorofores for the Photodetection and Photodynamic Therapy of Cancer (Fevrier, Lausanne, 2000), p. 20.
[27] A. P. Demchenko, Introduction to Fluorescence Sensing (Springer, Netherlands, 2009), p. 110.
[28] L. Gu, D. J. Hall, Z. Qin, E. Anglin, J. Joo, D. J. Mooney, S. B. Howell, and M. J. Sailor, Nature Commun. **4**, 2326 (2013).
[29] L. W. Zhang and N. A. Monteiro-Riviere, J. Biomed. Opt. **18**, 061214 (2013).
[30] A. C. Curry, M. Crow, and A. Wax, J. Biomed. Opt. **13**, 014022 (2008).
[31] E. Keedwell, Intelligent Bioinformatics: The Application of Artificial Intelligence Techniques to Bioinformatics Problems (Wiley, USA, 2005), p. 128.
[32] M. H. Hassoun, Fundamentals of Artificial Neural Networks (MIT Press, Cambridge, Massachusetts, 1995), p. 411.
[33] T. Dramiŕcanin, I. Zekoviŕc, B. Dimitrijeviŕc, S. Ribar, and M. D. Dramiŕcanin, Acta Phys. Pol. A **116**, 690 (2009).
[34] L. Lenhardt, I. Zekoviŕc, T. Dramiŕcanin, and M. D. Dramiŕcanin, Phys. Scr. **T157**, 014057 (2013).
[35] I. V. Gerdova, S. A. Dolenko, T. A. Dolenko, I. V. Churina, and V. V. Fadeev, Izv. Akad. Nauk Ser. Fiz. **66**, 1116 (2002).
[36] A. Ya. Chervonenkis, Problemy upravleniya **4**, 41 (2005).
[37] T. A. Dolenko, S. A. Burikov, A. M. Vervald, I. I. Vlasov, S. A. Dolenko, K. A. Laptinskiy, J. M. Rosenholm, and O. A. Shenderova, J. Biomed. Opt. **19**, 117007 (2014).
[38] S. A. Burikov, A. M. Vervald, I. I. Vlasov, S. A. Dolenko, K. A. Laptinskiy, and T. A. Dolenko, Opt. Mem. Neural Networks (Inf. Opt.) **22**, 156 (2013).
[39] A. A. Isakova, E. Yu. Krysanov, T. B. Demidova, M. V. Ivanova, A. V. Saphonov, and O. D. Omelchenko, in: Advanced Carbon Nanostructures International Conference, Book of Abstracts (The Ioffe Institute RAS, St. Petersburg, 2015), p. 106.
[40] D. N. Klyshko and V. V. Fadeev, Sov. Phys. Dokl. **23**, 55 (1978).

[41] T. Dolenko, S. Burikov, K. Laptinskiy, J. M. Rosenholm, O. Shenderova, and I. Vlasov, Phys Status Solidi A **212**, 2512 (2015).
[42] J. Xiao, P. Liu, L. Li, and G. Yang, J. Phys. Chem. C **119**, 2239 (2015).
[43] I. H. Witten, E. Frank, and M. A. Hall, Data Mining: Practical Machine Learning Tools and Techniques, 3rd ed. (Morgan Kaufmann, Amsterdam, 2011), p. 664.
[44] B. Strojny, N. Kurantowicz, E. Sawosz, M. Grodzik, S. Jaworski, M. Kutwin, M. Wierzbicki, A. Hotowy, L. Lipińska, and A. Chwalibog, Plos ONE **10**, e0144821 (2015).
[45] S. Rojas, J. Gispert, R. Martin, S. Abad, C. Menchón, D. Pareto, V. M. Víctor, M. Álvaro, H. García, and J. R. Herance, ACS Nano **5**, 5552 (2011).
[46] V. Paget, J. A. Sergent, R. Grall, S. Altmeyer-Morel, H. A. Girard, T. Petit, C. Gesset, M. Mermoux, P. Bergonzo, J. C. Arnault, and S. Chevillard, Nanotoxicology **8**, 46 (2014).
[47] Y. Zhu, J. Li, W. Li, Y. Zhang, X. Yang, N. Chen, Y. Sun, Y. Zhao, C. Fan, and Q. Huang, Theranostics **2**, 302 (2012).
[48] Y. Yuan, X. Wang, G. Jia, J.-H. Liu, T. Wang, Y. Gu, S.-T. Yang, S. Zhen, H. Wang, and Y. Liu, Diam. Relat. Mater. **19**, 291 (2010).